Noname manuscript No.
(will be inserted by the editor)

Comparison of Different Grid of Tags Detection Methods in Tagged Cardiac MR Imaging

Aymeric Histace · Christophe Portefaix · Bogdan Matuszewski

Received: date / Accepted: date

Abstract ***Purpose:*** Noninvasive imaging assessment of cardiac function is important in cardiovascular disease diagnosis, especially for evaluation of local cardiac motion. Tagged Cardiac MRI has been developed for this purpose, but evaluation of the results requires quantification and automation. ***Method:*** Two methods utilizing active contour modeling for wall motion extraction based on tagged cardiac MRI scans were evaluated based on properties of tracking methods in the image domain and frequency domain. Three criteria were used: accuracy, inter-subject and intra-subject sensitivity. The tracking results were evaluated by a medical expert. The evaluation methodology and its possible generalization to other diagnostic methods were considered. ***Results:*** Image-domain and frequency-domain analysis of tagged cardiac MRI data sets were evaluated demonstrating that the image domain method provides better results. The image-domain method method is much more resistant to changes in the data, this time, due to a different subject being scanned. The frequency domain approach is not suitable for clinical applications, as the global error is significantly increased (more than 20%). ***Conclusion:*** The image-domain method was found most effective, and it can generate a set of clearly identified parameters. The evaluation approach can be an interesting alternative to classical psychovisual studies which are time consuming and often fastidious for clinicians.

Keywords Tagged Cardiac MRI · Detection · Accuracy · Intra-subject sensitivity, · Inter-subject sensitivity.

A. Histace
ETIS UMR CNRS 8051, ENSEA-University of Cergy-Pontoise, 6 av. du Ponceau 95000, France
Tel.: +33(1)34256834
Fax: +33(1)34256920
E-mail: aymeric.histace@u-cergy.fr

C. Portefaix
CHU Reims, Maison Blanche Hospital, 51092 Reims Cedex, France

B. Matuszewski
ADSIP Research Center, University of Central Lancashire, Preston, UK

Introduction

The non invasive assessment of the cardiac function is of primary importance for the diagnosis and treatment of cardiovascular pathologies. Whereas the classical cardiac MRI only allows measurements of anatomical and global functional parameters of the myocardium such as mass, volume or ejection, tagged cardiac MRI [1] makes possible measurements of some cardiac functional parameters through the evaluation of the intra-myocardial displacement. For instance, this type of information improve characterization of the myocardium viability after an infarction helping, for example, in making decision about suitability of angioplasty or coronary surgery. Moreover, tagged cardiac MRI may also facilitate ischemia detection during stress studies and allow for the early detection of myocardial dysfunction with cardiomyopathies.

The SPAMM (SPAce Modulation of Magnetization) acquisition protocol [2,3] we used for the tagging of MRI data, displays a deformable, 45°-oriented, dark grid which follows the contraction (also referred as systole in the text) of myocardium as shown in temporal Short-Axis (SA) sequences (Figure 1). The temporal tracking of this grid makes the evaluation of the local intramyocardial displacement of the Left Ventricle (LV) possible.

Fig. 1 SA tagged MRI extracted from a sequence acquired all along systole of the LV.

Numerous studies were carried out focusing on the analysis of the deformations of the grid of tags on SA sequences: [4–25]. The most recent methods led to interesting clinical quantification of some specific parameters as local displacements or local deformations but remain hard to validate as these are not considered as standard parameters by medical experts, and are not clearly correlated to parameters, such as ejection, commonly used by clinicians.

We have presented in recent papers [26,27] two original approaches based on iterative deformations of a virtual grid of tags using active contours methodology. Both approaches led to satisfying results and overcame the classical drawbacks typically associated with the active contours, namely sensitivity to noise and difficulty with handling large displacements.

In this article, we present a study that has been done in collaboration with clinical cardiologists for the evaluation of both developed methods. This study is not based on a clinical trial involving a large number of volunteers. Indeed, whereas the classical cardiac MRI is a well established protocol for the study of global cardiac motion, the tagged cardiac MRI is still considered to be under development and as for such it is hard to conduct a large clinical study which involves a significative number of patients and specialists. Thus, instead of quantifying classical clinical parameters, to demonstrate

the potential of the methods, we propose to evaluate the detection of the tagging grid directly in the image domain using image processing assessment criteria.

Methods

Data

For this study 10 healthy volunteers aged between 25 and 35 years, have been scanned. The GE 1.5T MRI scanner was used (Genesis Signa GE Healthcare, Milwaukee, Wisc, UK) with gated fast-card gradient echo sequence (fgre sequence with the torso coil, TE= 5.4ms , TR=11ms , Flip Angle = 12°, Field of View = 400mm , Slice thickness = 10mm , Matrix : 256x256 with a reconstructed pixel size of 1.56/1.56) and SPAMM activated with tag spacing of 11mm. 12 SA slices, per subject, have been acquired on average with the exact number depending on the size of the subject's heart. Each acquisition sequence consists of 20 images from which 6 are sufficient for the complete temporal description of the LV contraction (referred t_1 to t_6 in the following). On average it took about half an hour per volunteer to complete the acquisition.

Detection of the grid

The general principle of both detection technics has already been described in [28, 26] and is shortly reviewed here: To detect the tagging grid on SA sequences, we iteratively deform a virtual grid (Fig. 2) modeled by B-spline functions and controlled by 44 nodes P located at the intersections of the grid lines. Each node has associated energy E, defined as the sum of two terms:

$$E = w_{internal}.E_{internal} + w_{external}.E_{external} \quad , \tag{1}$$

This energy is iteratively minimized leading to the alignment of the virtual grid with the grid present in the LV systole.

The internal energy, $E_{internal}$, imposes the regularity constraint on the whole grid in order to obtain a coherent result, e.g. without grid folding, reflected by the consistent spacing of the intersection point of the virtual grid. For further details, reader should refer to [18].

The external energy, $E_{external}$, is responsible for the accurate representation of the image grid lines by the virtual grid. To achieve this, the information about grid position in the noisy image must be somehow extracted so it can be compared, by the $E_{external}$, against evolving virtual grid. Number of different methods have been proposed since 1988 to extract this tag information. In this paper, we propose to compare the two methods already mentioned in the introduction section. For the first method $E_{external}$ is computed in the frequency domain [26], whereas for the second this energy is computed in the image domain thanks to an adapted grid restoration approach utilizing selective diffusion [27].

For each method the tagging grid has been detected and tracked for different values of the $\frac{w_{internal}}{w_{external}}$ (Eq. (1)). It is important to note that the $\frac{w_{internal}}{w_{external}}$ ratio is a function of the spatial image coordinates. The value of this ratio must be optimized for parts of the image representing LV to ensure a good tracking performance. Outside LV only the internal term of Eq. (1) is taken into account. Inside the LV cavity, where the grid

quickly fades because of blood ejection, $E_{internal}$ is tuned separately in order to assure that the corresponding point converge to the center of the LV cavity since the study focuses on the LV contraction. Labeling of each nodes is automatically made thanks to an original tracking of the epicardial and endocardial boundaries described in [29].

Optimal tuning of the $\frac{w_{internal}}{w_{external}}$ ratio for the nodes located within myocardium can be seen as the main problem for the obtaining of good detection results (see Fig. 3 for illustration).

Statistical study description

The proposed approach for evaluation of detection methods is based on a statistical study performed by a medical expert with 15 years of experience in cardiovascular imaging.

The automatic detection of the grid is performed on a complete sequence, subsequently the expert counts the number of pixels of the virtual grid which are considered well positioned with respect to the real tags present in image. To make this counting easier, the calculated grid for each phase and slice of a given sequence is shown as red colored lines (see Fig. 4 for illustration).

Only the pixels of the virtual grid inside the myocardium are taken into account for the statistical study. The rest of the pixels (outside myocardium and within the cardiac cavity) do not have clinical meaning and would biased the statistical study if they were taken into account. To help the expert this discrimination step, the nodes of the virtual tagging grid which are within myocardium are automatically colored in green (see Fig. 2) [29]. The quality of automatic grid detection is measured as a percentage of all the correctly localized tags in the myocardium, as assessed by the clinical expert.

Due to the small width of real tag lines (3 pixels), following the clinical expert advice, the threshold determining if a tag has been correctly localized has been set to a single pixel. This low value is justified by the fact that in particular pathologies (like akinesia for example) the real tagging grid merely moves. Thus, even a small error of detection can lead to wrong conclusions. An example of well and badly detected tags is shown in Fig.4.

The comparison between the two methods is based on their potential to obtain good detection results in terms of percentage of correctly detected tags within the myocardium for a given value of the $\frac{w_{internal}}{w_{external}}$ ratio. The assessment criteria used in this study are detailed below.

Accuracy, intra- and inter- subject sensitivity

The main objective of this study was to perform comparison of the tag detection methods from the perspective of their suitability for real clinical applications. It is therefore important to consider clinical experts expectations with respect to the obtained results such as computation time, accuracy as well as intra- and inter- subject sensitivity.

The average computation time can be easily quantified. We estimate that it takes about 5 minutes to process the complete SA sequence, for both frequency and image domain methods, using the latest generation of desktop computers. This computation time can certainly be shortened by further optimized implementation using for example general purpose GPUs. Current implementation is based on the PV-WAVE 8.0 from Visual Numerics Society.

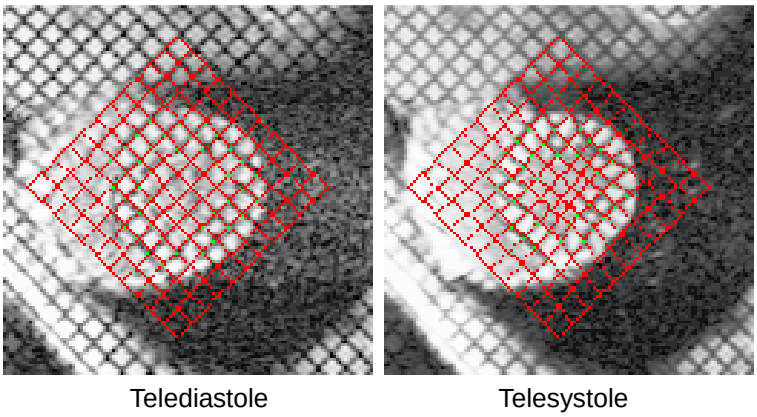

Fig. 2 General principle of the developed methods for the detection of the tagging grid in SA cardiac slice. A virtual deformable grid modeled using B-splines is superimposed on the image to the left ventricular area. Each node of the virtual grid has an energy E (Eq. (1)). The virtual grid is aligned with the tagging grid present in the image through iterative minimization of the energy E.

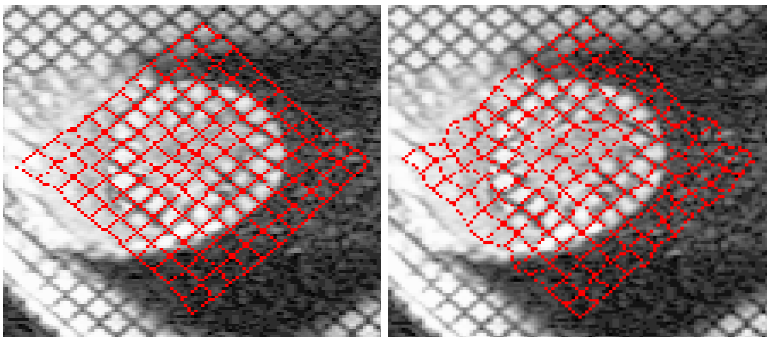

Fig. 3 Tagging grid detection error for the frequency domain method, the optimal result is shown on the left whereas result corresponding to 10% variation of the $\frac{w_{internal}}{w_{external}}$ from its optimal value is shown on the right.

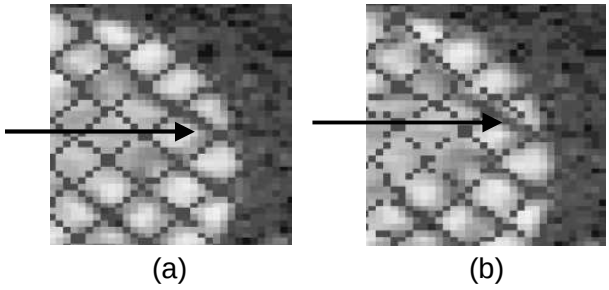

Fig. 4 Example of well and badly detected grid. (a) the arrow points at a set of grid pixels that can be considered as well detected. (b) the arrow points at the same set of pixels but badly detected this time as the virtual grid is placed away from these pixels.

The accuracy, intra- and inter- subject sensitivity are defined as follows:

- *Accuracy:* As defined in [30], accuracy is the "degree to which a measurement is true or correct". In [31], accuracy is defined as "the difference between observed values and theoretical values, i.e., known from a ground truth". This is illustrated in Fig. 4. In the proposed here framework the automatically detected virtual grid in each image is interpreted as observations whereas the manual segmentation performed by the expert is considered as corresponding to the true (or theoretical) representation. Based on this definition evaluation of the methods' accuracy consists of finding the best value of the $\frac{w_{internal}}{w_{external}}$ ratio which minimizes the percentage of wrongly detected pixels within the myocardium. This value of $\frac{w_{internal}}{w_{external}}$ is also used as a reference value for the quantification of methods' inter- and intra- patient sensitivity.

- *intra-subject sensitivity:* this parameter refers to the possible distortion of results obtained from the automatic tag detection due to data variability intrinsic to a specific subject. This data variability might for example be due to different subject position during successive scans.
  For the specific application considered in this paper, the intra-subject sensitivity is measured indirectly as the grid detection error express as a function of the $\frac{w_{internal}}{w_{external}}$ ratio averaged over all scans acquired for different subject. In practice to assess the intra-subject sensitivity the optimal $\frac{w_{internal}}{w_{external}}$ is calculated first separately for all the scans. Subsequently these values are changed and the averaged detection errors are recalculated as the function of the percentage change of the $\frac{w_{internal}}{w_{external}}$. When a method exhibit low intra-subject sensitivity the level of the detection error for a given subject does not depend strongly on the $\frac{w_{internal}}{w_{external}}$. In such a case the value of this parameter can be selected only in few iterations based on a single scan and subsequently kept unchanged during the successive acquisitions preformed for the same patient.

- *inter-subject sensitivity:* this parameter quantifies sensitivity of the grid detection results obtained for different subjects. Similarly to the intra-subject sensitivity the inter-subject sensitivity is defined based on the $\frac{w_{internal}}{w_{external}}$ ratio. This time though the changes in the detection error are measured for results obtained for different subject with the fixed value of the ratio. In practice the optimal value of the $\frac{w_{internal}}{w_{external}}$ is calculated separately for each subject. Subsequently the average detection error is calculated for results obtained for different subject with the value of the ratio unchanged. The selection of the optimal value of the $\frac{w_{internal}}{w_{external}}$ could be time consuming process. The low value of the inter-subject sensitivity suggest that the same value of this ratio can be used for different subject leading to simplified grid detection methodology.

Results

Accuracy

To estimate accuracy of both methods, a reference sequence was arbitrarily chosen

	Detection errors				
Slice level	**Apex 1**	**Apex 2**	**Mid ventricular**	**Base 1**	**Base 2**
Pixels in myocardium	290	275	275	300	300
Contraction phase					
t1	5	0	0	5	5
t2	0	0	0	5	5
t3	5	10	10	0	15
t4	5	5	20	0	10
t5	0	5	20	10	10
t6	5	15	20	10	20
Mean error	**1,14%**	**2,12%**	**4,24%**	**1,67%**	**3,61%**
Standard Deviation	**2,58**	**5,85**	**9,83**	**4,47**	**5,85**

Table 1 Detection errors obtained using frequency domain method on the reference sequence for the optimal value of $\frac{w_{internal}}{w_{external}} = 2$.

	Detection errors				
Slice level	**Apex 1**	**Apex 2**	**Mid ventricular**	**Base 1**	**Base 2**
Pixels in myocardium	290	275	275	300	300
t1	5	0	0	5	5
t2	0	0	0	5	5
t3	5	10	10	0	15
t4	5	5	10	0	10
t5	0	5	15	5	10
t6	5	10	20	10	10
Mean error	**1,14%**	**1,82%**	**3,33%**	**1,39%**	**3,06%**
Standard Deviation	**2,58**	**4,47**	**8,01**	**3,76**	**3,76**

Table 2 Detection errors obtained using image domain method on the reference sequence for the optimal value of $\frac{w_{internal}}{w_{external}} = 2$.

by the expert from the available ten. The $\frac{w_{internal}}{w_{external}}$ ratio was then empirically tuned in order to obtain the most accurate detection results in terms of minimum percentage of wrongly detected pixels within myocardium.

Optimal results on the reference sequence, with the medical expert evaluating the results from the automatic grid detection algorithm, are shown in Tab. 1 for the frequency domain approach and Tab. 2 for the image domain method.

It can be noticed from Tabs. 1 and 2, the global detection error is relatively small for both approaches with the estimated (within the myocardium) optimal empirical value of $\frac{w_{internal}}{w_{external}}$ equal to two. Indeed, the global error remains lower or just above 4% for each slice. The biggest error value is encountered at the mid ventricular slice where displacements are the most important. The expert grouped the badly detected pixels in a multiple of 5, what means that when detection errors are made, all five pixels describing the virtual line of the grid between two particular nodes were considered as wrongly detected by the expert.

To visually confirm these detection results, an example of the grid detection obtained on the mid ventricular slice of the reference sequence are shown in Fig. 5 for the frequency domain approach and in Fig. 6 for the image domain method.

Intra-subject sensitivity

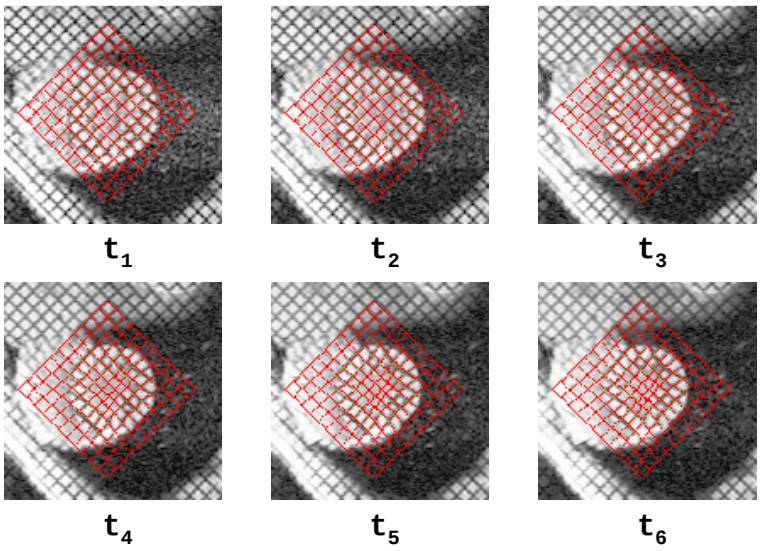

Fig. 5 Detection of the tagging grid using frequency domain approach on SA images taken from the reference sequence obtained for the optimal value of $\frac{w_{internal}}{w_{external}} = 2$.

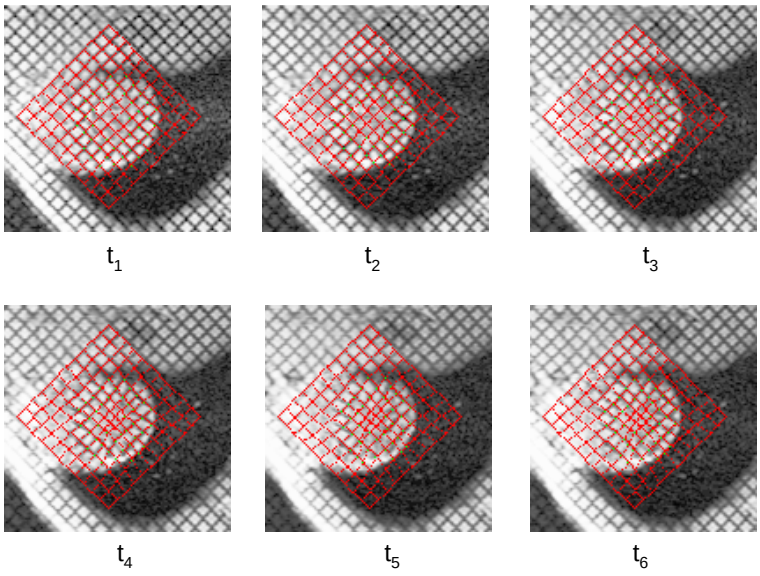

Fig. 6 Detection of the tagging grid using image domain approach on SA images taken from the reference sequence obtained for the optimal value of $\frac{w_{internal}}{w_{external}} = 2$.

Fig. 7 and Fig. 8 show the average global detection error for each slice, expressed in percentages as a function of the variation of the $\frac{w_{internal}}{w_{external}}$ ratio from the empirically estimated optimal value.

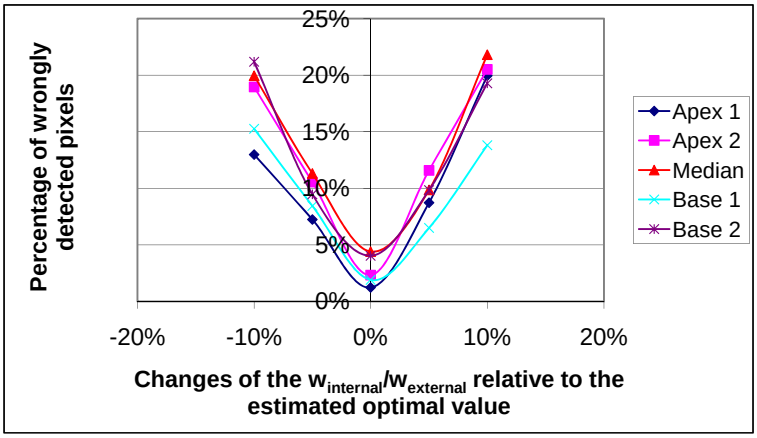

Fig. 7 The global detection error as a function of the $\frac{w_{internal}}{w_{external}}$ ratio for the frequency domain approach.

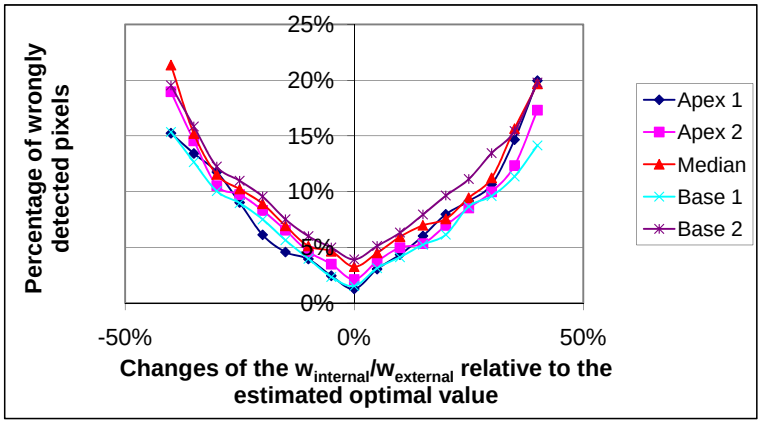

Fig. 8 The global detection error as a function of the $\frac{w_{internal}}{w_{external}}$ ratio for the image domain approach.

Although it can be seen that accuracy for both, frequency and image domain methods, depends on the value of the $\frac{w_{internal}}{w_{external}}$ ratio, this dependence for the former is much more stronger than for the later. For example, assuming that 10% detection accuracy is acceptable, the use of the frequency approach would require selection of the $\frac{w_{internal}}{w_{external}}$ ratio with 5% accuracy, whereas the use of the image domain approach would mean that clinicians can be up to 6 times less accurate about selection of this parameter, as

	Detection errors				
Slice level	**Apex 1**	**Apex 2**	**Mid ventricular**	**Base 1**	**Base 2**
Pixels in myocardium	275	275	290	290	290
t1	5	0	10	5	5
t2	5	5	15	10	15
t3	20	25	30	20	20
t4	30	50	50	45	55
t5	45	75	75	90	105
t6	60	105	95	90	100
Mean error	**10,00%**	**15,15%**	**16,38%**	**12,64%**	**17,24%**
Standard Deviation	**22,08**	**38,43**	**36,98**	**34,82**	**44,05**

Table 3 The global detection error for frequency domain method and sequences different from the reference, using the optimal value of the $\frac{w_{internal}}{w_{external}}$ from the reference sequence.

	Detection errors				
Slice level	**Apex 1**	**Apex 2**	**Mid ventricular**	**Base 1**	**Base 2**
Pixels in myocardium	275	275	290	290	290
t1	5	5	0	5	5
t2	5	0	0	5	5
t3	5	5	10	0	10
t4	0	5	5	5	10
t5	0	5	15	5	5
t6	10	5	10	5	10
Mean error	**1,52%**	**1,52%**	**2,30%**	**1,44%**	**2,59%**
Standard Deviation	**3,76**	**2,04**	**6,06**	**2,04**	**2,74**

Table 4 The global detection error for image domain method and sequences different from the reference, using the optimal value of the $\frac{w_{internal}}{w_{external}}$ from the reference sequence.

30% deviation from the optimal value will still guarantee that the detection error will not exceed 10%.

Inter-subject sensitivity

To check the performance of the investigated methods for different subjects, the expert assessed the accuracy of both methods on sequence different from the reference sequence but with the optimal value of $\frac{w_{internal}}{w_{external}}$ estimated for the reference sequence. The corresponding results are shown in Tab. 3 and Tab. 4.

As in the previous section the image domain method provides better results. This method is much more resistant to changes in the data, this time, due to a different subject being scanned. The frequency domain approach is not suitable for clinical applications, as the global error is significantly increased (more than 20%) without a the re-tuning of the $\frac{w_{internal}}{w_{external}}$ ratio. This significant increased in the error can also be seen in Fig. 9 where the miss-alignment between virtual grid and tags is visible especially at the end of the diastole (t_6). Contrary to the frequency domain, the image domain method have low inter-subject sensitivity as seen in Tab. 4, as the error is always smaller than 3%. Consequently, the image domain method appears to be more suitable for a clinical use since no tuning of the $\frac{w_{internal}}{w_{external}}$ ratio is necessary to maintain a high detection accuracy.

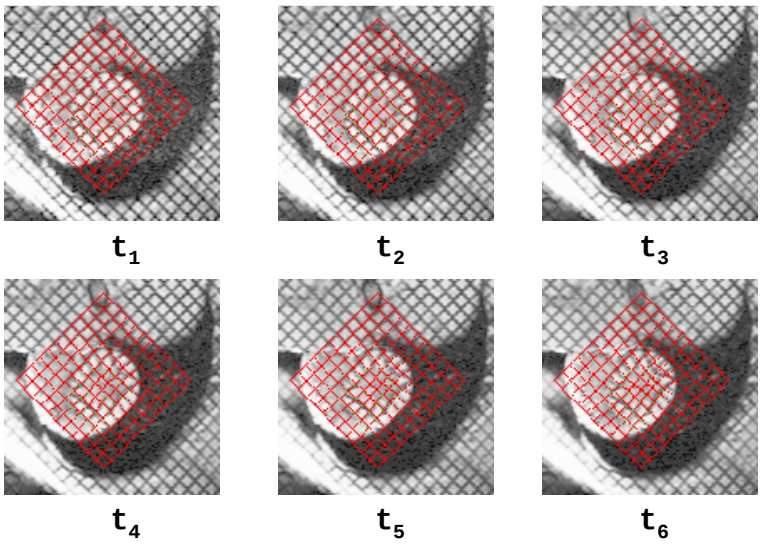

Fig. 9 Detection of the tagging grid using the frequency domain approach for a subject different from the reference, but with the optimal value of $\frac{w_{internal}}{w_{external}}$ calculated from the reference sequence. It can be noticed that the virtual grid appears not to match well tagging grid in the myocardium area.

Considering the results presented in previous sections, it is now possible to perform a global evaluation of the detection error for the whole set of acquired sequences (10 volunteers). This evaluation has been made only for the image domain method which is, as it has been shown above, more suitable for clinical applications. For this part of the study, not only the medical expert performed the statistical study on the whole set of ten data sets, but also two non-medical expert (but Image Processing (IP) expert) performed the same task in order to evaluate the inter-operator variability. The results of this experiment are presented in Fig. 10.

As it can be noticed, the global error remains low (below 4%) for each volunteer and is in agreement with the results obtained by the expert on the reference sequence. Moreover, on the whole set of images, the highest global error is only of 3.39%. Furthermore all results obtained from all the observers (medical expert and IP experts) differ by no more 0.5%, and therefore provide some confidence about accuracy of the quoted above results.

Discussion

Quantification of local displacements of the myocardium is of primary importance for the diagnosis and follow-up of cardiomyopathies. Tagged cardiac MRI is able to provide that kind of quantification but it remains hard to compare different methods proposed in the literature for processing such data. In this paper, we proposed to make this comparison easier by evaluating the algorithms properties directly in the image

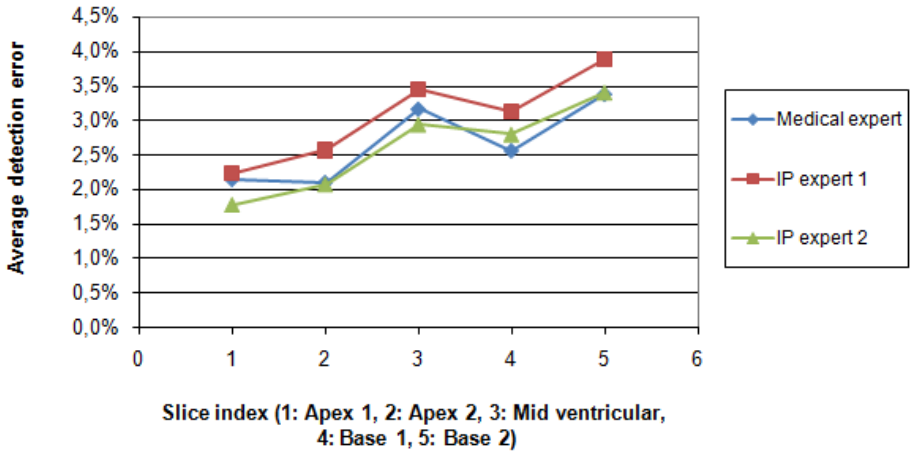

Fig. 10 The mean global error (expressed in percentages) calculated for the image domain method and averaged over ten data sets. For each volunteer, global error is calculated as the mean of the errors characterizing each phase at a given slice level. The $\frac{w_{internal}}{w_{external}}$ ratio had the fix value of 2 for all the data sets.

domain. For illustration, two different methods, previously proposed by authors, were compared using the proposed methodology. For each of these methods three parameters were assessed: accuracy, intra-subject sensitivity and inter-subject sensitivity.

The accuracy results show that both approaches for the detection of the tagging grid are accurate enough for further quantitative evaluation of clinical parameters (Figs. 5 and 6).

The inter-subject sensitivity, as defined in the methods section, shows a significant difference between the tested methods, with the image domain method outperforming frequency domain method. The proposed assessment methodology was able to clearly highlight important difference in the performance of both methods.

The study also has shown that intra-subject sensitivity, as defined in the methods section, is an important assessment parameter for the discrimination of particular methods aiming at the detection of the tagging grid.

Although the proposed three parameters have been sufficient for the discrimination of the tested methods, it is an open question what are the optimal parameters for studies, particularly when more methods are being compared. To get closer to an answer the authors currently collaborate with other researchers who have also developed such tools for the analysis of tagged cardiac MRI. A future study based on the comparison of more than two methods should give important insight for further developments of the statistical studies.

Due to a time consuming nature of the manual evaluation of the detection results, the whole set of experiment has not been repeated for a different reference frame. Having said this the results of inter-subject sensitivity gives us some confidence that the obtained results would be similar if a different reference data were to be selected.

The presented results seem not to be significantly biased due to number of experts or amount of data used. The whole data set contained scans from ten subjects with 30 images per subject giving in total 300 images for which detection accuracy was evaluated. This in our opinion is big enough data set to average out any errors due to

outliers. The results are also not too much influenced by a subjectivity of the expert as the similar results where obtained for two non-experts. This can be explained by the fact that the statistical method we propose is above all linked to image processing and does not need the critical clinical knowledge as in the classical clinical validation protocol. It is important to highlight that the goal of this study is to propose an alternative to classical clinical parameter quantification by making a statistical comparison of tracking methods in terms of image processing criteria. As a consequence, it can be noticed that even a person with only basic knowledge about morphology of the LV can perform this statistical study.

At this stage of the study, it would be difficult to conclude that the presented validation protocol can be adapted for comparison of other approaches developed for tagged MRI analysis. Once again, a study involving more different techniques is needed. In any such study though it appears essential to clearly identify one or more key-parameters that will be used as reference hyper-parameters for global evaluation and comparison. As a consequence, only methods which have the same hyper-parameter(s) can be compared. This can clearly be seen as a limitation of our method.

Nevertheless, clinically speaking, the proposed approach can facilitate identification of the most interesting developed methods for the tracking of the grid in tagged cardiac MRI. As a consequence, performances of more different types of methods for local quantitative estimation of the LV function can be foreseen. Currently, some new acquisition technics have shown capabilities for ischemia early diagnosis, like the Strain-Encoded technic (known as SENC) [32,33] for instance. In this context, it becomes of primary importance to be able to clearly identify which type of methods are valuable to compare among themselves for this type of early diagnosis (tagged MRI, SENC acquisition or more generally high resolution tagging technics) in order to be efficient. We think that the method proposed in this article can be of some valuable help for the achievement of this task by making possible a early selection of the tag tracking methods which are of real interests for clinical application and which deserve to be integrated within a large-scale comparison study of automatic LV function estimation.

Conclusion

This paper presents a method for comparison of grid detection techniques in the tagged cardiac MRI sequences. The properties of the proposed methodology have been demonstrated on two particular methods developed previously by the authors. It has been shown that protocol based on the quantification of accuracy, intra-subject sensitivity and inter-subject sensitivity, which are defined in the paper, provide a tool for validation of a given method and enable a comparison with other techniques without the need for a complete clinical study. The proposed three parameters appear to be discriminating enough to show meaningful differences between two methods based on the same fundamental principle.

The method proposed here is an interesting alternative to usual validation methods which appear not to be suitable for the analysis of tagged cardiac MRI sequences, since no “gold standard” parameters can be easily correlated with the local displacement and deformation parameters usually estimated with help of this particular imaging modality.

References

1. E. Zerhouni, D. Parish, W. Rogers, A. Yang, and E. Shapiro, "Human heart : tagging with MR imaging - a method for noninvasive assessment of myocardial motion," *Radiology*, vol. 169, no. 1, pp. 59–63, 1988.
2. L. Axel and L. Dougherty, "MR imaging of motion with spatial modulation of magnetization," *Radiology*, vol. 172, no. 2, pp. 349–350, 1989.
3. L. Axel and L. Dougherty, "Improved method of spatial modulation of magnetization (spamm) for mri of heart wall motion," *Radiology*, vol. 172, pp. 349–350, 1989.
4. J.L. Prince and E. McVeigh, "Motion estimation from tagged MR image sequences," *IEEE Transactions on Medical Imaging*, vol. 11, no. 2, pp. 238–249, 1992.
5. S. Kumar and D. Goldgof, "Automatic tracking of SPAMM grid and the estimation of deformation parameters from cardiac MR images," *IEEE Transactions on Medical Imaging*, vol. 13, no. 1, pp. 122–132, 1994.
6. S. Gupta and J. Prince, "On variable brightness optical flow for tagged MRI," in *Information Processing in Medical Imaging*, Kluwer, Ed., Dordrecht (Pays-Bas), 1995, pp. 323–334, Kluwer.
7. D. Kraitchman, A. Young, C. Chang, and L. Axel, "Semi-automatic tracking of myocardial motion in MR tagged images," *IEEE Transactions on Medical Imaging*, vol. 14, no. 3, pp. 422–433, 1995.
8. A.A. Young, D.L. Kraitchmann, L. Dougherty, and L. Axel, "Tracking an finite element analysis of stripe deformation in magnetic resonance tagging," *IEEE Transactions on Medical Imaging*, vol. 14, no. 3, pp. 413–421, 1995.
9. S. Zhang, M. Douglas, L. Yaroslavsky, R. Summers, V. Dilsizian, L. Fananapazir, and S. Bacharach, "A fourier based algorithm for tracking SPAMM tags in gated magnetic resonance cardiac images," *Medical Physics*, vol. 32, no. 8, pp. 1359–1369, 1996.
10. S. Gupta, J. Prince, and S. Androutsellis-Theotokis, "Bandpass optical flow for tagged MRI," in *International Conference on Image Processing*, San Diego CA, 1997, vol. 3, pp. 364–367.
11. M. Guttman, E. Zerhouni, and E. McVeigh, "Analysis of cardiac function from MR images," *IEEE Computer Graphics and Applications*, vol. 17, no. 1, pp. 30–38, 1997.
12. P. Radeva, A. Amini, and J. Huang, "Deformable B-solids and implicit snakes for 3D localization and tracking of SPAMM MRI data," *Computer Vision and Image Understanding*, vol. 66, pp. 163–178, 1997.
13. A.A. Amini, Y. Chen, R.W. Curwen, V. Mani, and J. Sun, "Coupled B-snake grids and constrained thin-plate splines for analysis of 2D tissue deformations from tagged MRI," *IEEE Transaction on Medical Imaging*, vol. 17, no. 3, pp. 344–356, 1998.
14. T. Denney, "Estimation and detection of myocardial tags in MR images without user-defined myocardial contours," *IEEE Transactions on Medical Imaging*, vol. 18, no. 4, pp. 330–344, 1999.
15. L. Dougherty, J. Asmuth, A. Blom, L. Axel, and R. Kumar, "Validation of an optical flow method for tag displacement estimation," *IEEE Transactions on Medical Imaging*, vol. 18, no. 4, pp. 359–363, 1999.
16. M. Groot-Koerkamp, G. Snoep, A. Muijtjens, and G. Kemerink, "Improving contrast and tracking of tags in cardiac magnetic resonance images," *Magnetic Resonance in Medicine*, vol. 41, pp. 973–982, 1999.
17. N.F. Osman, E.R. Mc Veigh, and J.L. Prince, "Imaging heart motion using Harmonic Phased MRI (HARP)," *IEEE Transactions on Medical Imaging*, vol. 19, pp. 186–202, 2000.
18. S. Urayama, T. Matsuda, N. Sugimoto, S. Mizuta, N. Yamada, and C. Uyama, "Detailed motion analysis of the left ventricular myocardium using an MR tagging method with a dense grid," *Magnetic Resonance in Medicine*, vol. 44, no. 73-82, 2000.
19. P. Clarysse, L. Bracoud, P. Croisille, and I.E. Magnin, "Integrated quantitative analysis of tagged magnetic resonance images," *FIMH-LNCS*, vol. 2230, pp. 69–75, 2001.
20. I. Haber, R. Kikinis, and C.F. Westin, "Phase-driven finite elements model for spatio-temporal tracking in tagged mri," in *Proceedings of Fourth International Conference On Medical Image Computing and Computer Assisted Intervention (MICCAI'01)*, 2001, pp. 1352–1353.
21. R. Chandrashekara, R.H. Mohiaddin, and D. Rueckert, "Analysis of myocardial motion in tagged MR images using nonrigid image registration," in *Medical Image Understanding and Analysis*, Porthmouth, 2002.

22. C. Petitjean, N. Rougon, F. Prêteux, Ph. Cluzel, and Ph. Grenier, "A non rigid registration approach for measuring myocardial contraction in tagged mri using exclusive f-information," in *Proceedings International Conference on Image and Signal Processing (ICISP'2003), Agadir, Morocco*, 25-27 June 2003.
23. N. Rougon, C. Petitjean, F. Prteux, P. cluzek, and P. Grenier, "A non-rigid registration approach for quantifying myocardial contraction in tagged MRI using generalized information measures," *Medical Image Analysis*, vol. 9, pp. 353–375, 2005.
24. E. Oubel, M. De Craene, M. Gazzola, A.O. Hero, and A.F. Frangi, "Multiview registration of cardiac tagging mri images," in *Biomedical Imaging: From Nano to Macro, 2007. ISBI 2007. 4th IEEE International Symposium on*, 2007, pp. 388–391.
25. L. Axel, Sohae Chung, and Ting Chen, "Tagged mri analysis using gabor filters," in *Biomedical Imaging: From Nano to Macro, 2007. ISBI 2007. 4th IEEE International Symposium on*, 2007, pp. 684–687.
26. A. Histace, C. Cavaro-Ménard, V. Courboulay, and M. Ménard, "Analysis of tagged cardiac MRI sequences," *Lecture Notes on Computer Science (Proceedings of the 3rd Functional Imaging and Modelling of the Heart (FIMH) Workshop)*, vol. 3504, pp. 404–413, June 2005.
27. A. Histace, M. Ménard, and C. Cavaro-Ménard, "Selective diffusion for oriented pattern extraction: Application to tagged cardiac MRI enhancement," *Pattern Recognition Letters*, vol. 30, no. 15, pp. 1356–1365, 2009.
28. A. Histace, L. Hermand, and C. Cavaro-Mnard, "Tagged cardiac MR images analysis," in *Biosignal 2002*, June 2002, pp. 313–315.
29. A. Histace, B. Matuszewski, and Y. Zhang, "Segmentation of myocardial boundaries in tagged cardiac mri using active contours: a gradient-based approach integrating texture analysis," *International Journal of Biomedical Imaging*, vol. 2009, pp. 8 pages, 2009.
30. C.S. Goodman, *Introduction to health care technology assessment*, National Library Medecine/NICHSR, 1998.
31. P. Jannin, J.M. Fitzpatrick, D.J. Hawkes, X. Pennec, Shahidi R., and M.W. Vannier, "Validation of medical image processing in image-guided therapy," *IEEE Transactions on Medical Imaging*, vol. 21, no. 12, pp. 1445–1449, December 2002.
32. M. Neizel, D. Lossnitzer, G. Korosoglou, T. Schaufle, H. Peykarjou, H. Steen, C. Ocklenburg, E. Giannitsis, H.A. Katus, and N.F. Osman, "Strain-encoded MRI for evalutation of left ventricular function and transmurality in acute myocardial infarction," *Circ Cardiovasc Imaging*, vol. 2, no. 2, pp. 116–122, 2009.
33. G. Korosoglou, D. Lossnitzer, D. Schellberg, A. Lewien, A. Wochele, T. Schaeufele, M. Neizel, H. Steen, E. Giannitsis, H.A. Katus, and N.F. Osman, "Strain-encoded cardiac MRI as an adjunct for dobutamine stress testing: incremental value to conventional wall motion analysis," *Circ Cardiovasc Imaging*, vol. 2, no. 2, pp. 132–140, 2009.